Chemical Science

ROYAL SOCIETY OF CHEMISTRY

EDGE ARTICLE

View Article Online
View Journal | View Issue

Cite this: *Chem. Sci.*, 2023, **14**, 5340

All publication charges for this article have been paid for by the Royal Society of Chemistry

Received 16th February 2023
Accepted 24th April 2023

DOI: 10.1039/d3sc00881a

rsc.li/chemical-science

Unveiling the impact of oxidation-driven endogenous protein interactions on the dynamics of amyloid-β aggregation and toxicity†

Zhi Du,‡[aj] Eunju Nam,‡[a] Yuxi Lin,‡[b] Mannkyu Hong,[ac] Tamás Molnár,[d] Ikufumi Kondo,[e] Koichiro Ishimori,[ef] Mu-Hyun Baik,[ac] Young-Ho Lee*[bghi] and Mi Hee Lim*[a]

Cytochrome *c* (Cyt *c*), a multifunctional protein with a crucial role in controlling cell fate, has been implicated in the amyloid pathology associated with Alzheimer's disease (AD); however, the interaction between Cyt *c* and amyloid-β (Aβ) with the consequent impact on the aggregation and toxicity of Aβ is not known. Here we report that Cyt *c* can directly bind to Aβ and alter the aggregation and toxicity profiles of Aβ in a manner that is dependent on the presence of a peroxide. When combined with hydrogen peroxide (H_2O_2), Cyt *c* redirects Aβ peptides into less toxic, off-pathway amorphous aggregates, whereas without H_2O_2, it promotes Aβ fibrillization. The mechanisms behind these effects may involve a combination of the complexation between Cyt *c* and Aβ, the oxidation of Aβ by Cyt *c* and H_2O_2, and the modification of Cyt *c* by H_2O_2. Our findings demonstrate a new function of Cyt *c* as a modulator against Aβ amyloidogenesis.

Introduction

Alzheimer's disease (AD) is a neurodegenerative disorder that causes memory loss and cognitive impairment.[1–3] A major pathological hallmark of AD is the deposition of senile plaques primarily composed of amyloid-β (Aβ) aggregates. Aβ self-assembles to generate oligomers, protofibrils, and amyloid fibrils.[3–5] Among various Aβ species, structured oligomers are reported to be toxic, with the ability to directly and indirectly disturb intracellular and extracellular systems.[4] Specifically, Aβ oligomers can induce oxidative damage, including lipid peroxidation by membrane permeabilization, while oxidative stress can increase Aβ production by activating β-secretase.[6–8] This process propagates a circular cascade of Aβ accumulation and oxidative damage. Recent studies suggest that the intertwined networks associated with Aβ and cellular components lead to the complicated pathological nature of AD.[3] Metal ions, such as Cu(I/II) and Zn(II), bind to Aβ peptides, modify their aggregation pathways, and stabilize toxic structured oligomers.[9,10] Furthermore, the overproduction of reactive oxygen species (ROS) triggered by dysregulated redox-active metal ions bound and unbound to Aβ results in oxidative stress with the subsequent impact towards neuronal death.[11,12]

Cytochrome *c* (Cyt *c*) is a globular protein that contains 104 amino acid residues with a covalently attached heme group as a cofactor.[13] Cyt *c* exerts different functions depending on its cellular localization and conditions and, thus, plays the pleiotropic role in biological systems.[14] In general, Cyt *c* serves as an electron shuttle in the mitochondrial respiratory chain as well as a scavenger against ROS.[15] In addition to mitochondria, Cyt *c* is also found in the cytosol and is associated with cell differentiation and proliferation.[15] Moreover, extracellular Cyt *c* is reported to promote the survival of hypoxic neurons.[16] Under oxidative stress, Cyt *c* is released from mitochondria to the cytosol.[13,14] When the concentration of cytosolic Cyt *c* exceeds the threshold, apoptosis initiates through activating caspases and exhibiting its peroxidase-like activity.[15,17] Aβ is proposed to trigger the efflux of Cyt *c* from mitochondria to the cytosol and,

[a]*Department of Chemistry, Korea Advanced Institute of Science and Technology (KAIST), Daejeon 34141, Republic of Korea. E-mail: miheelim@kaist.ac.kr*

[b]*Research Center for Bioconvergence Analysis, Korea Basic Science Institute (KBSI), Ochang, Chungbuk 28119, Republic of Korea. E-mail: mr0505@kbsi.re.kr*

[c]*Center for Catalytic Hydrocarbon Functionalizations, Institute for Basic Science (IBS), Daejeon 34141, Republic of Korea*

[d]*Department of Biochemistry, Institute of Biology, Eötvös Loránd University, H-1117 Budapest, Hungary*

[e]*Graduate School of Chemical Sciences and Engineering, Hokkaido University, Kita 13, Nishi 8, Kita-ku, Sapporo 060-8628, Japan*

[f]*Department of Chemistry, Faculty of Science, Hokkaido University, Kita 10, Nishi 8, Kita-ku, Sapporo 060-0810, Japan*

[g]*Bio-Analytical Science, University of Science and Technology (UST), Daejeon 34113, Republic of Korea*

[h]*Graduate School of Analytical Science and Technology, Chungnam National University, Daejeon 34134, Republic of Korea*

[i]*Research Headquarters, Korea Brain Research Institute (KBRI), Daegu 41068, Republic of Korea*

[j]*Department of Biomedical Engineering, College of Biomedical Engineering, Taiyuan University of Technology, Taiyuan 030024, PR China*

† Electronic supplementary information (ESI) available. See DOI: https://doi.org/10.1039/d3sc00881a

‡ These authors contributed equally to this work.

consequently, cause oxidative stress and apoptosis.[18,19] Based on these findings, the reactivities of Cyt *c* with Aβ have been recently explored.[20–22] For example, Cyt *c* significantly attenuated ROS generated by the Aβ–heme complexes *via* direct electron transfer.[20] Studies with Aβ mutants and Cyt *c* exhibited that metal-free Aβ and metal-bound Aβ have distinct electrostatic interactions with Cyt *c*.[21] The mechanism of how Cyt *c* affects the pathology associated with Aβ is not known to date, however.

We questioned whether Cyt *c* directly interacts with Aβ and modifies its aggregation and toxicity profiles. Thus, we evaluated the impact of Cyt *c* on the aggregation of both metal-free Aβ and metal-bound Aβ under normal conditions and oxidative stress as well as the cytotoxicity of the resultant Aβ species. Mechanistic details in the distinct reactivity of Cyt *c* towards Aβ amyloidogenesis in the absence and presence of ROS, including their contacts, conformational changes, and oxidative modifications, were probed. Overall, our work illuminates a novel modulative role of Cyt *c* in the Aβ-related pathology of AD.

Results and discussion

Effects of Cyt *c* on the aggregation of metal-free and metal-bound $A\beta_{42}$ with and without ROS

The influence of Cyt *c* on the aggregation of metal-free $A\beta_{42}$ in the absence and presence of H_2O_2 used as a ROS was first monitored by gel electrophoresis with western blotting

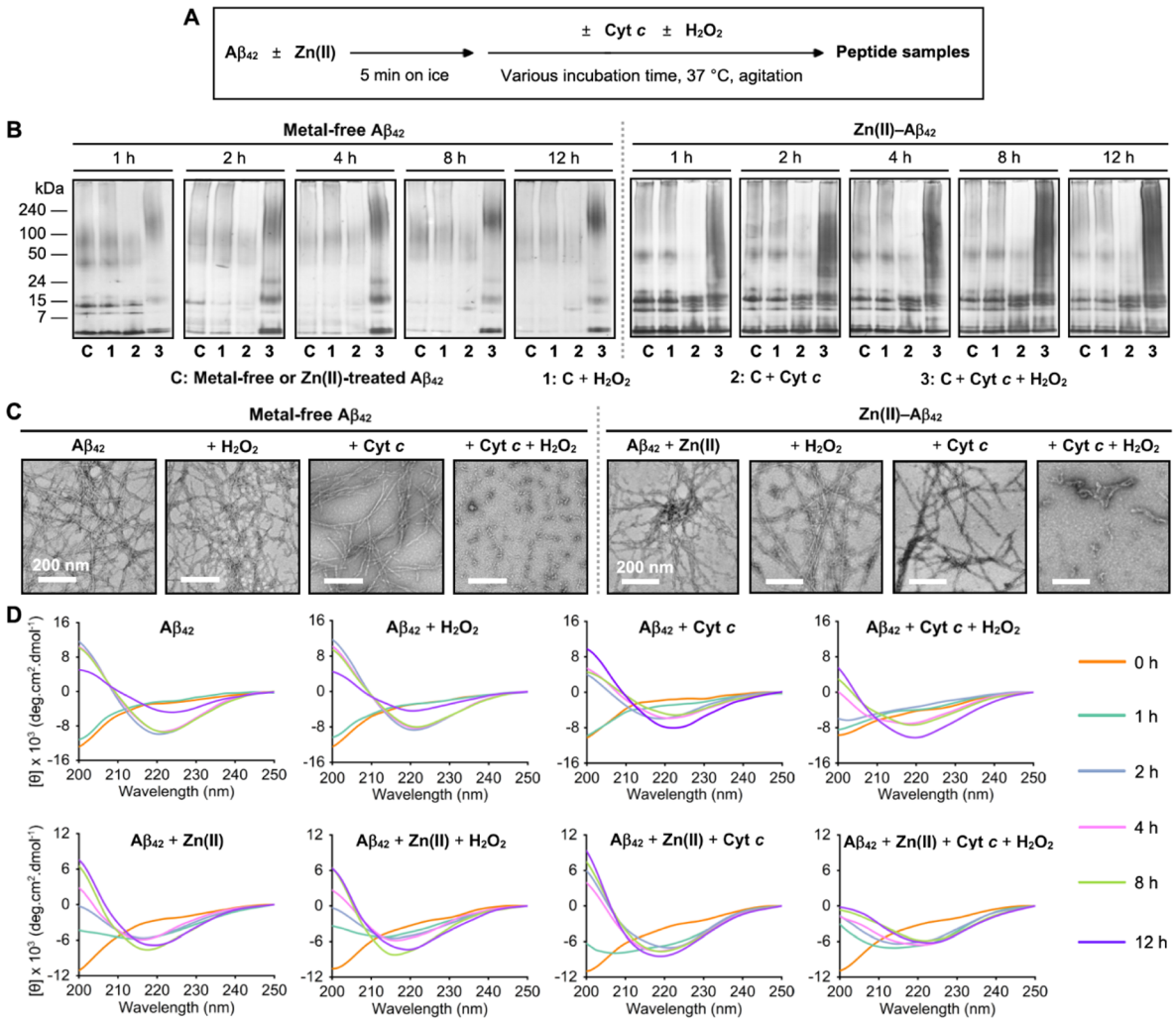

Fig. 1 Effects of Cyt *c* on the aggregation of metal-free and Zn(II)-bound $A\beta_{42}$ in the absence and presence of H_2O_2. (A) Scheme of $A\beta_{42}$ aggregation experiments with and without Zn(II). (B) Size distribution of the resultant $A\beta_{42}$ species at various incubation time points analyzed by gel/western blot using an anti-Aβ antibody (6E10). (C) Morphology of the peptide aggregates produced after 12 h incubation visualized by TEM. Scale bars = 200 nm. Conditions: $[A\beta_{42}] = 25\ \mu M$; $[Zn(II)] = 25\ \mu M$; [Cyt *c*] = 25 μM; $[H_2O_2] = 200\ \mu M$; 150 mM HEPES, pH 7.4; 37 °C; constant agitation (250 rpm). (D) Change in the secondary structures of metal-free and Zn(II)-treated $A\beta_{42}$ upon aggregation in the presence of Cyt *c* and H_2O_2 observed by CD spectroscopy. $A\beta_{42}$ was incubated with either Cyt *c*, H_2O_2, or both for 0, 1, 2, 4, 8, and 12 h. The spectra of $A\beta_{42}$ with Cyt *c* were obtained by subtracting the features of Cyt *c* under the same conditions. In 20 mM sodium phosphate (NaPi), pH 7.4, 150 mM NaF that was chosen to avoid the optical interference from the buffer, the aggregation behavior of $A\beta_{42}$ was similar to that in the HEPES buffer (Fig. S1†). Conditions: $[A\beta_{42}] = 40\ \mu M$; $[Zn(II)] = 40\ \mu M$; [Cyt *c*] = 4 μM; $[H_2O_2] = 200\ \mu M$; 20 mM NaPi, pH 7.4, 150 mM NaF; 37 °C; constant agitation (250 rpm).

(gel/western blot) using an anti-Aβ antibody (6E10) to determine the molecular weight (MW) distribution of the resultant Aβ species, as described in Fig. 1A and B. The band intensities observed in low MWs of $A\beta_{42}$ species in a range of *ca.* 4–15 kDa were weakened upon incubation, indicative of its aggregation. When $A\beta_{42}$ was treated with Cyt *c*, the aggregation of $A\beta_{42}$ was accelerated showing the disappearance of overall bands after 2 h incubation. Distinct from $A\beta_{42}$ with and without Cyt *c*, an increased amount of $A\beta_{42}$ species ranging from 100 to 240 kDa and the bands at low MWs (*ca.* 4–24 kDa) were observed upon treatment of $A\beta_{42}$ with both Cyt *c* and H_2O_2. The size distribution of $A\beta_{42}$ was not significantly changed by H_2O_2 only. Furthermore, the morphology of $A\beta_{42}$ aggregates produced with either Cyt *c*, H_2O_2, or both was visualized by transmission electron microscopy (TEM). As depicted in Fig. 1C, the samples of $A\beta_{42}$ with and without H_2O_2 showed long and thin fibrils after 12 h incubation. When $A\beta_{42}$ was incubated with Cyt *c*, long and thick fibrils were detected. Notably, the addition of both Cyt *c* and H_2O_2 led the generation of amorphous $A\beta_{42}$ aggregates as well as short and flexible protofibrils. Therefore, these results support that Cyt *c* can alter the aggregation of $A\beta_{42}$ in the absence and presence of H_2O_2 to different extents. It should be noted that the impact of Cyt *c* on the aggregation kinetics of $A\beta_{42}$ was not observed by a fluorescent assay because of its signal interference.

To verify the conformational change of $A\beta_{42}$ upon treatment of either Cyt *c*, H_2O_2, or both, the samples were further analyzed by circular dichroism (CD) spectroscopy. We measured the far-UV CD spectra of $A\beta_{42}$ incubated with Cyt *c* in an $A\beta_{42}$-to-Cyt *c* ratio of 10 : 1 that was selected to limit Cyt *c*'s signals. At this stoichiometry, Cyt *c* could affect the aggregation of $A\beta_{42}$ (Fig. S2†). As shown in Fig. 1D and S3,† the CD spectra of $A\beta_{42}$ species with or without H_2O_2 upon incubation exhibited a single negative peak at *ca.* 220 nm, indicative of the formation of amyloid fibrils, and an increase in the β-sheet content to *ca.* 46%. Neither Cyt *c* nor H_2O_2 significantly influenced the change in the secondary structures of $A\beta_{42}$. Different from $A\beta_{42}$ with and without either Cyt *c* or H_2O_2, $A\beta_{42}$ added with both of them formed the β-sheet structure in a slower manner. The overall results obtained by gel/western blot, TEM, and CD measurements manifest that Cyt *c* can alter the size distribution, morphology, and secondary structures of $A\beta_{42}$ upon aggregation in a peroxide-dependent manner.

As metal ions affect the aggregation of Aβ *via* coordination to Aβ forming metal-bound Aβ (metal–Aβ) complexes,[1,2,9,10] we additionally assessed the impact of Cyt *c* on the aggregation of Zn(II)–$A\beta_{42}$ with and without H_2O_2, as illustrated in Fig. 1A and B. It should be noted that we did not probe how Cyt *c* affects the aggregation of Cu(II)–$A\beta_{42}$ in a peroxide-dependent manner because the reaction of Cu(II) with H_2O_2 interferes with our analysis.[5] The sample containing Zn(II)–$A\beta_{42}$ and Cyt *c* indicated a decrease in the amount of $A\beta_{42}$ aggregates (*ca.* 24 to 240 kDa) upon incubation. When Zn(II)–$A\beta_{42}$ was treated with both Cyt *c* and H_2O_2, the smearing in a range of 4–240 kDa was visualized in the gel, which was different from those from the samples of Zn(II)–$A\beta_{42}$ with and without addition of either Cyt *c* or H_2O_2. As shown in Fig. 1C, a mixture of short and flexible protofibrils and amorphous aggregates was detected by incubation of Zn(II)–$A\beta_{42}$ with both Cyt *c* and H_2O_2, compared to long fibrils produced by Zn(II)–$A\beta_{42}$ with and without either Cyt *c* or H_2O_2. As expected, the sample of Zn(II)–$A\beta_{42}$ with Cyt *c* and H_2O_2 exhibited the reduced β-sheet content to *ca.* 24%, relative to that of Zn(II)–$A\beta_{42}$ only or Zn(II)–$A\beta_{42}$ with either Cyt *c* or H_2O_2 (*ca.* 40%), as illustrated in Fig. 1D and S4.† These observations confirm the formation of less structured $A\beta_{42}$ aggregates. Collectively, our aggregation investigations corroborate that Cyt *c* can vary the aggregation behaviors of both metal-free $A\beta_{42}$ and Zn(II)-bound $A\beta_{42}$ with and without H_2O_2 to different extents. Particularly, Cyt *c* accelerates the aggregation of $A\beta_{42}$ in the absence of H_2O_2 and redirects Aβ peptides into off-pathway less structured assemblies when H_2O_2 is present.

Complexation between Cyt *c* and $A\beta_{42}$

To illuminate how Cyt *c* affects the aggregation of $A\beta_{42}$, the direct interactions between Cyt *c* and $A\beta_{42}$ were first analyzed by electrospray ionization-mass spectrometry (ESI-MS), a soft ionization method for characterizing protein complexes.[23] As depicted in Fig. 2B, new peaks at 1688 and 1878 *m*/*z* corresponding to the complex between Cyt *c* and $A\beta_{42}$ with +10 and +9 charge states, respectively, were detected upon treatment of $A\beta_{42}$ with Cyt *c*. The Cyt *c*–$A\beta_{42}$ adduct in a 1 : 1 ratio was mainly observed, with the complexes with the Cyt *c*-to-Aβ ratios of 1 : 2 and 2 : 1 (Fig. S5†). The binding of Cyt *c* to $A\beta_{42}$ was further investigated by isothermal titration calorimetry (ITC), as shown in Fig. S6.† An endothermic ITC isotherm was obtained and the ITC peak intensity decreased as Cyt *c* was titrated into the solution of $A\beta_{42}$, indicating their intermolecular interactions. The ITC peaks exhibited the two components, *i.e.*, the early sharp peak and the late broad peak. The broad ITC peaks may be attributed to the aggregation of $A\beta_{42}$ by Cyt *c*, which would be further boosted because of rigorous stirring in an ITC cell. The ITC measurements revealed a heat change resulting from both Cyt *c*–$A\beta_{42}$ interaction and $A\beta_{42}$ aggregation, which would hamper the accurate fitting analysis to obtain thermodynamic parameters for intermolecular interactions.

Next, the binding properties of Cyt *c* with $A\beta_{42}$ were probed by two-dimensional (2D) nuclear magnetic resonance (NMR) spectroscopy employing either ^{15}N-labeled $A\beta_{42}$ or Cyt *c*. As presented in Fig. 2C, when Cyt *c* was added into uniformly ^{15}N-labeled $A\beta_{42}$, moderate chemical shift perturbations (CSPs) were detectable near or in the self-recognition and *C*-terminal regions of $A\beta_{42}$ (*e.g.*, Glu11, Lys16, Val18, Val39, and Ile41), respectively, that are critical for Aβ aggregation.[2] To further analyze the binding site of Cyt *c* towards $A\beta_{42}$, we employed ^{15}N-labeled Cyt *c* with 104 amino acid residues that were expressed and purified as previously described.[24] Upon incubation of ^{15}N-labeled Cyt *c* with $A\beta_{42}$, CSPs were indicated at several amino acid residues of Cyt *c*, including Gly1, Asp2, Lys5, Gly6, Lys8, Ile11, His18, Gly34, Phe36, Thr40, Tyr46, Leu68, Lys72, and Ile95, as displayed in Fig. 2D and S7.† This suggests that $A\beta_{42}$ has multiple contacts onto the whole region of Cyt *c*. It should be noted that no significant differences in the CSPs or signal intensity of ^{15}N-labeled $A\beta_{42}$ were observed over 12 h incubation

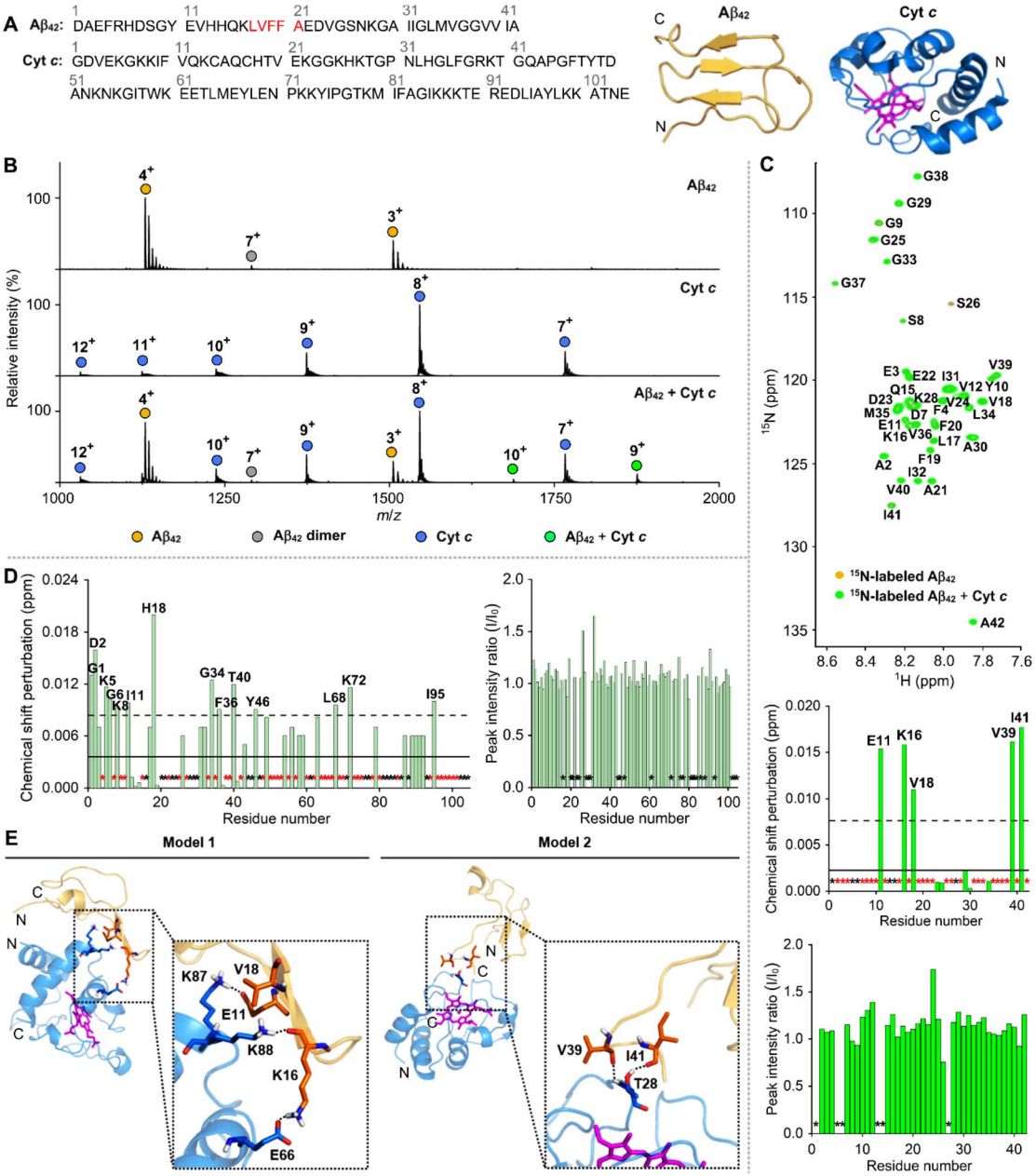

Fig. 2 Interaction between Cyt *c* and Aβ$_{42}$. (A) Amino acid sequences and structures of Cyt *c* (PDB 1HRC)[28] and Aβ$_{42}$.[29] The heme group in Cyt *c* and the self-recognition site of Aβ$_{42}$ are highlighted in pink and red, respectively. (B) Complexation between Cyt *c* and Aβ$_{42}$ detected by ESI-MS. Conditions: [Aβ$_{42}$] = 100 μM; [Cyt *c*] = 100 μM; 20 mM ammonium acetate, pH 7.4; 37 °C; incubation for 30 min. The samples were diluted by 10-fold prior to injection to the mass spectrometer. (C) Two-dimensional (2D) ^{1}H–^{15}N band-selective optimized flip angle short transient-heteronuclear multiple quantum correlation (SOFAST-HMQC) NMR spectra (800 MHz) of ^{15}N-labeled Aβ$_{42}$ monomer with and without Cyt *c*. The average of chemical shift perturbations (CSPs) and the average plus one standard deviation are presented with solid and dashed lines, respectively. Black asterisks represent the amino acid residues that cannot be resolved for analysis, and red asterisks indicate the amino acid residues without detectable CSPs. Conditions: [^{15}N-labeled Aβ$_{42}$] = 40 μM; [Cyt *c*] = 200 μM; 150 mM HEPES, pH 7.4; 10% v/v D_2O; 10 °C. (D) Analysis of the CSPs and the change in the peak intensity observed within ^{15}N-labeled Cyt *c* by addition of Aβ$_{42}$. The 2D ^{1}H–^{15}N heteronuclear single quantum coherence (HSQC) NMR spectra of ^{15}N-labeled Cyt *c* with and without Aβ$_{42}$ monomer are depicted in Fig. S7.† (E) Representative models of the Cyt *c*–Aβ$_{42}$ interfaces from the trajectories of MD simulations. Initial conformations of Cyt *c* (PDB 1HRC; blue)[28] and Aβ$_{42}$ (yellow)[29] were used for binding studies. The heme group in Cyt *c* is highlighted in pink. Model 1 and 2 of the Cyt *c*–Aβ$_{42}$ adducts are illustrated in Fig. S9.† Possible hydrogen bonds are depicted with dashed black lines.

(Fig. S8†), indicating that insoluble aggregates did not form under our experimental conditions.

The structural heterogeneity of intrinsically disordered Aβ limits the experimental determination of high-resolution local and global conformations. Molecular dynamics (MD) simulations guided by experimental data can present a detailed picture for protein–protein interactions.[25–27] To investigate the potential binding modes of Cyt *c* to Aβ$_{42}$, MD simulations were carried out

with an X-ray crystal structure of Cyt *c* (PDB 1HRC)[28] and an $A\beta_{42}$ conformer acquired from the MD simulation data,[29] as shown in Fig. 2A. Two possible Cyt *c*–$A\beta_{42}$ dimeric interfaces associated with two majorly interacting regions (*e.g.*, Glu11, Lys16, and Val18; Val39 and Ile41) of $A\beta_{42}$ were shown in 2D NMR studies (Fig. 2E and S9†). It should be noted that our MD simulations did not consider the CSPs in Cyt *c* obtained upon addition of $A\beta_{42}$ because they were detected in most of its amino acid residues. The model on the left involves Glu11, Lys16, and Val18 close to the self-recognition site in $A\beta_{42}$ as the major binding region with Cyt *c*. The carboxylate group of Glu11 forms a hydrogen bond with a length of 1.9 Å against the side chain of Lys87 in Cyt *c*. Furthermore, the side chain of Lys16 in $A\beta_{42}$ interacts with Glu66 in Cyt *c* in an average length of 1.9 Å and its backbone carbonyl group exhibits an additional hydrogen bond with Lys88 in Cyt *c*. The hydrophobic Val18 residue of $A\beta_{42}$ resides between two positioned alkyl chains of the aforementioned Lys87 and Lys88 in Cyt *c*. In the other probable model, Thr28 in Cyt *c* plays a key role in interacting with the *C*-terminal region of $A\beta_{42}$ that is anchored to Cyt *c* by the following two hydrogen bonds: (i) the backbone carbonyl group of Val39 in $A\beta_{42}$ and the backbone amide moiety of the Thr28 in Cyt *c*; (ii) the backbone carbonyl group of Ile41 in $A\beta_{42}$ and the side chain hydroxyl group of Thr28 in Cyt *c*. It should be noted that we chose the initial structure of $A\beta_{42}$ for MD simulations from conformational ensembles identified based on a combination of experimental and theoretical data.[29] The monomeric $A\beta_{42}$ structure, which occupied the largest population in the conformational ensembles, was selected as a template. Although the initial structure of $A\beta_{42}$ can influence the trajectories and results of MD simulations, our computational results may provide valuable insights into the molecular interaction between Cyt *c* and $A\beta_{42}$. Overall, our ESI-MS, ITC, NMR, and computational studies support that Cyt *c* can interact with $A\beta_{42}$ in a direct but relatively weak binding manner.

Oxidation of $A\beta_{42}$ by Cyt *c* and H_2O_2

Given that ROS cause oxidative modifications of proteins and, consequently, alter their structures and functions,[30] we evaluated whether Cyt *c* could oxidize $A\beta_{42}$ in the presence of H_2O_2. Like other heme-containing peroxidases, Cyt *c* with H_2O_2 can catalytically oxidize a wide range of substrates *via* high-valent Fe(IV) intermediates.[31] The peroxidase-like activity of Cyt *c* was measured by the ABTS assay [ABTS = 2,2′-azinobis(3-ethylbenzthiazoline-6-sulfonate)].[32] Cyt *c* with H_2O_2 noticeably induced the oxidation of ABTS in a concentration- and time-dependent manner while H_2O_2 was not able to significantly oxidize ABTS under our experimental conditions, which suggests its peroxidase-like activity (Fig. S10†).

Moving forward, we probed the oxidation of $A\beta_{42}$ in the presence of both Cyt *c* and H_2O_2 by ESI-MS. The peaks at 1133, 1137, and 1139 *m*/*z*, assigned to be $[A\beta_{42} + O + 4H]^{4+}$, $[A\beta_{42} + 2O + 4H]^{4+}$, and $[A\beta_{42} + Na + O + 3H]^{4+}$, respectively, were detected, as displayed in Fig. 3A. The peak intensities associated with oxidized $A\beta_{42}^{4+}$ species produced by Cyt *c* and H_2O_2 were enhanced, compared to those by H_2O_2 only. To identify the oxidation sites of $A\beta_{42}$ by both Cyt *c* and H_2O_2, tandem MS ($ESI\text{-}MS^2$) with collision-induced dissociation (CID) was performed. A mass shift of 16 Da from y_8 and b_{14}, as presented in Fig. 3B and C, indicated that both His14 and Met35 could be oxidized. Oxidized $A\beta_{42}^{4+}$ by H_2O_2 at 1133 *m*/*z* exhibited Met35 as the oxidation site according to a mass shift of 16 Da from b_{35} and y_8, as depicted in Fig. 3D. Moreover, in the case of Zn(II)-added $A\beta_{42}$, the oxidation sites of $A\beta_{42}$ by both Cyt *c* and H_2O_2 were identical with those illustrated above (Fig. S11†). These observations regarding Aβ oxidation are consistent with previous reports regarding oxidative modifications onto the Met and His residues in Aβ species isolated from amyloid plaques.[33,34] The Met35 residue in Aβ is highly susceptible to the oxidation to sulfoxide or sulfone forms upon exposure to H_2O_2.[35,36] Oxidized Met35 can alter the solubility, aggregation, and cytotoxicity of Aβ *via* decreasing the hydrophobicity of its *C*-terminal region and varying its secondary structures.[35–37] It

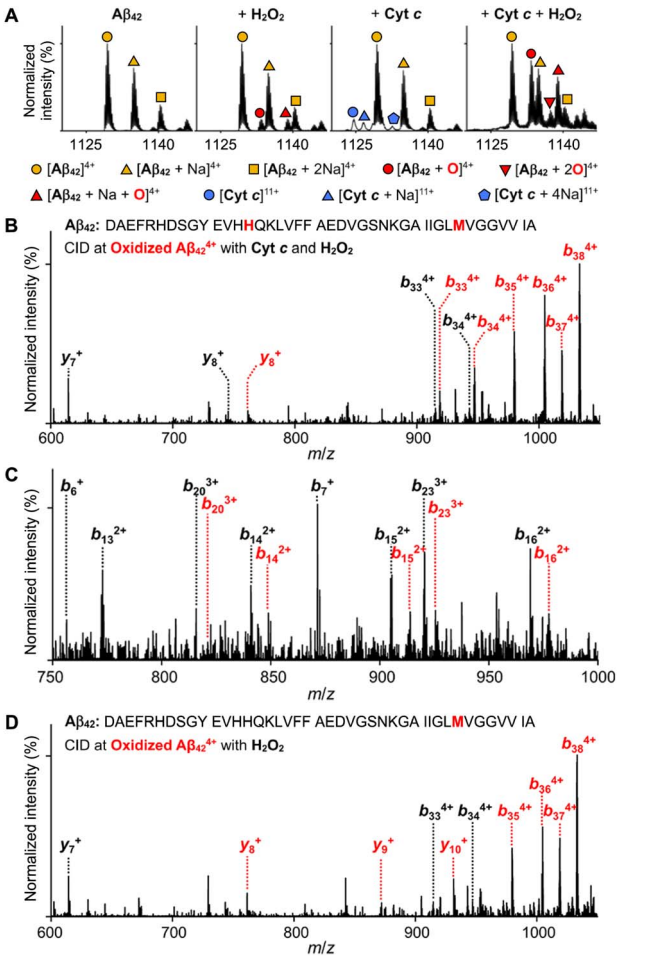

Fig. 3 Oxidation of $A\beta_{42}$ in the presence of Cyt *c* and H_2O_2 analyzed by ESI-MS and $ESI\text{-}MS^2$. (A) ESI-MS spectra of +4-charged $A\beta_{42}$ treated with either Cyt *c*, H_2O_2, or both. Oxidized $A\beta_{42}^{4+}$ obtained upon treatment with both Cyt *c* and H_2O_2. [(B) 1133 *m*/*z* (oxidized $A\beta_{42}^{4+}$); (C) 1139 *m*/*z* (an adduct of oxidized $A\beta_{42}^{4+}$ with Na^+)] were analyzed by $ESI\text{-}MS^2$. (D) $ESI\text{-}MS^2$ spectrum of oxidized $A\beta_{42}^{4+}$ produced by H_2O_2. Conditions: $[A\beta_{42}] = 100$ μM; [Cyt *c*] = 100 μM; $[H_2O_2] = 1.6$ mM; 20 mM ammonium acetate, pH 7.4; 37 °C; incubation for 30 min; without agitation. The 10-fold diluted samples were injected to the mass spectrometer.

should be noted that H_2O_2 did not significantly affect Aβ aggregation under our experimental conditions with a concentration of H_2O_2 (200 μM), which was much lower than that used for previous studies (*ca.* 12 mM).[35] Additionally, the His14 residue participates in Zn(II) binding of Aβ and is oxidized to 2-oxo-histidine,[5–7,32,38] which may contribute to the modulative reactivity of Cyt *c* with H_2O_2 against the aggregation of Zn(II)–Aβ. Together, our studies confirm that Cyt *c* significantly triggers oxidative modifications of both metal-free Aβ and Zn(II)–Aβ in the presence of H_2O_2, which consequently affects their aggregation profiles.

Modification of Cyt *c* by H_2O_2

H_2O_2 is reported to induce the oxidative modifications and conformational fluctuations of Cyt *c*, which ultimately enhances

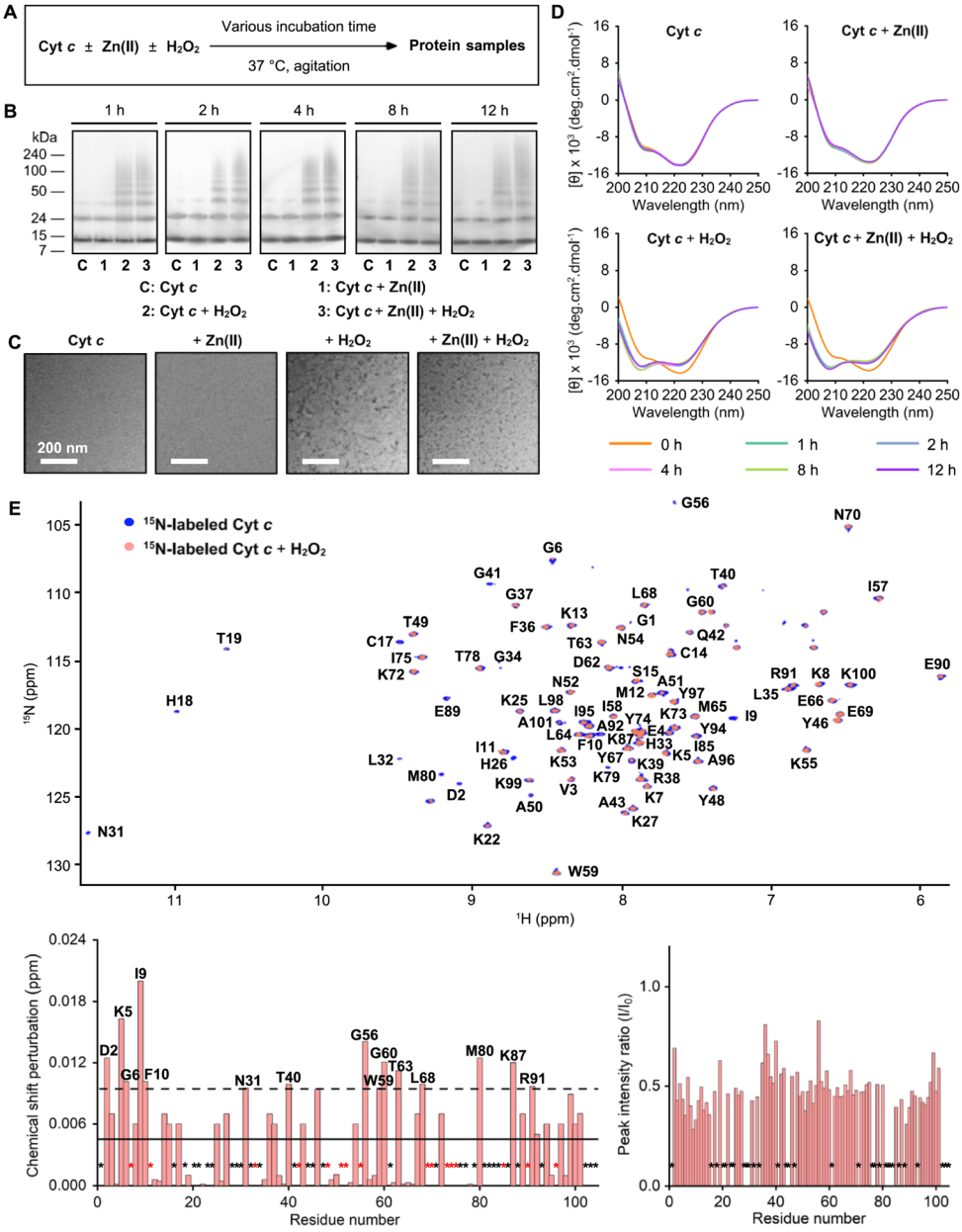

Fig. 4 Aggregation of Cyt *c* induced by H_2O_2. (A) Scheme of the aggregation experiments. (B) Size distribution of the resultant Cyt *c* species after incubation for 1, 2, 4, 8, and 12 h analyzed by gel/western blot using an anti-Cyt *c* antibody. (C) Morphology of Cyt *c* aggregates produced over 12 h incubation visualized by TEM. Scale bars = 200 nm. Conditions: [Cyt *c*] = 25 μM; [Zn(II)] = 25 μM; [H_2O_2] = 200 μM; 150 mM HEPES, pH 7.4; 37 °C; constant agitation (250 rpm). (D) Change in the secondary structures of Cyt *c* upon aggregation in the presence of Zn(II) and H_2O_2 monitored by CD spectroscopy. Cyt *c* was incubated with either Zn(II), H_2O_2, or both for 0, 1, 2, 4, 8, and 12 h. Conditions: [Cyt *c*] = 40 μM; [Zn(II)] = 40 μM; [H_2O_2] = 320 μM; 20 mM NaPi buffer, pH 7.4, 150 mM NaF; 37 °C; constant agitation (250 rpm). (E) 2D ^{1}H–^{15}N HSQC NMR spectra (800 MHz) of ^{15}N-labeled Cyt *c* with and without H_2O_2. The average of CSPs and the average plus one standard deviation are depicted with solid and dashed lines, respectively. Black asterisks represent the amino acid residues that cannot be resolved for analysis, and red asterisks indicate the amino acid residues without detectable CSPs. Conditions: [^{15}N-labeled Cyt *c*] = 20 μM; [H_2O_2] = 160 μM; 20 mM HEPES, pH 7.4; 10% v/v D_2O; 10 °C.

its peroxidase-like activity and triggers its aggregation.[39–41] We questioned whether H_2O_2 triggers the aggregation of Cyt *c* under our experimental conditions with the consequent impact on the aggregation of metal-free and Zn(II)-bound $A\beta_{42}$. Thus, the size distribution, morphology, and change in the secondary structures of the resultant Cyt *c* species upon incubation were analyzed by gel/western blot, TEM, dynamic light scattering (DLS), and CD spectroscopy, as summarized in Fig. 4 and S12–S16.† In the samples of Cyt *c* with H_2O_2 regardless of the presence of Zn(II), the smearing bands in the gels ranging from *ca.* 35 to 240 kDa were observed within 1 h, indicative of the formation of its aggregates, with the bands at *ca.* 12 and 24 kDa corresponding to monomeric and dimeric Cyt *c*, as illustrated in Fig. 4B. Additionally, amorphous Cyt *c* aggregates were visualized by TEM when Cyt *c* was added with H_2O_2 (Fig. 4C). Moreover, the hydrodynamic radius (R_H) of the resultant Cyt *c* species was determined by DLS. In the samples of Cyt *c* without H_2O_2 in both the absence and presence of Zn(II), the DLS peaks were centered at the R_H of *ca.* 1.7 nm, which is similar to the size of monomeric Cyt *c* reported in the previous study (Fig. S12 and S13†).[42] DLS data also showed no significant change in the R_H value over 12 h incubation, indicating that Cyt *c* did not aggregate without H_2O_2. In the case of the samples of Cyt *c* and H_2O_2 with and without Zn(II), however, new peaks with the R_H values larger than 100 nm were observed after 1 h incubation (Fig. S14 and S15†). Upon 12 h of incubation, two peaks were detected in the DLS profile. One peak was centered at *ca.* 7 nm, while the other was centered at 300–400 nm. These results suggest a heterogeneous distribution of Cyt *c* aggregates. We further examined the samples upon incubation by CD spectroscopy. The far-UV CD spectra of samples containing Cyt *c* and H_2O_2 with and without Zn(II) exhibited significant changes, as depicted in Fig. 4D. Structural analyses of the CD spectra revealed a decrease in the α-helical content from *ca.* 36% to *ca.* 29%, while the amount of random coil increased from *ca.* 30% to *ca.* 40%, as shown in Fig. S16,† consistent with the previous report.[31] Collectively, our results obtained by gel/western blot, TEM, DLS, and CD spectroscopy suggest the formation of amorphous Cyt *c* aggregates in the presence of H_2O_2 with and without Zn(II). Note that the treatment of both metal-free $A\beta_{42}$ and Zn(II)–$A\beta_{42}$ without H_2O_2 did not induce the aggregation of Cyt *c* (Fig. S17†).

The effect of H_2O_2 on the structural alteration of Cyt *c* was further investigated by 2D ^1H–^{15}N NMR spectroscopy. As presented in Fig. 4E, upon addition of H_2O_2 into ^{15}N-labeled Cyt *c*, moderate CSPs of Asp2, Lys5, Gly6, Ile9, Phe10, Asn31, Thr40, Gly56, Trp59, Gly60, Thr63, Leu68, Met80, Lys87, and Arg91 were observed. Furthermore, H_2O_2 significantly decreased the overall peak intensity of Cyt *c*, which could be resulted from the H_2O_2-mediated generation of amorphous NMR-invisible Cyt *c* aggregates. When ^{15}N-labeled Cyt *c* was incubated with both H_2O_2 and $A\beta_{42}$, the Asp2, Ile9, Lys27, Lys39, Thr40, Gly56, and Arg91 residues indicated relatively significant CSPs, compared to those with H_2O_2 only (Fig. S18†). H_2O_2 and $A\beta_{42}$ greatly enhanced the peak intensity of several amino acid residues, indicating that $A\beta_{42}$ can interact with amorphous Cyt *c* aggregates. It should be noted that no substantial difference in the CSP and signal intensity of ^{15}N-labeled $A\beta_{42}$ was observed by treatment of H_2O_2 (Fig. S19A†), in good agreement with the conclusion drawn from our gel/western blot, TEM, and CD measurements. Upon treatment of Cyt *c* and H_2O_2, the Asp23 and Gly29 residues of ^{15}N-labeled $A\beta_{42}$ were subject to greater CSPs, as depicted in Fig. S19B.† The peak intensity was also noticeably reduced, which may be caused by the co-aggregation of $A\beta_{42}$ and Cyt *c*.

To determine whether amorphous Cyt *c* aggregates and native Cyt *c* modify the aggregation of $A\beta_{42}$ in a distinct manner, we prepared amorphous Cyt *c* aggregates by incubating Cyt *c* with H_2O_2 for 12 h, as illustrated in Fig. S20A.† After incubation with preformed amorphous Cyt *c* aggregates, the change in the band intensity of monomeric $A\beta_{42}$ over time was different from that with or without native Cyt *c* (Fig. S20B†). In addition, the smearing in a range of 50–240 kDa indicated the distinct influence of amorphous Cyt *c* aggregates on $A\beta_{42}$ aggregation, relative to that of Cyt *c* with and without H_2O_2, which was also confirmed by morphological variations observed from TEM (Fig. S20C†). These observations manifest that the modification of Cyt *c* triggered by H_2O_2 was another driving force for modifying $A\beta_{42}$ aggregation.

Influence of Cyt *c* and H_2O_2 on the cytotoxicity induced by metal-free $A\beta_{42}$ and Zn(II)–$A\beta_{42}$

To evaluate the cytotoxicity of metal-free and Zn(II)-added $A\beta_{42}$ species produced by the addition of Cyt *c* and H_2O_2, we conducted the MTT assay [MTT: 3-(4,5-dimethylthiazol-2-yl)-2,5-diphenyltetrazolium bromide] employing a human neuroblastoma SH-SY5Y cell line. For the cell viability assay, we prepared metal-free and Zn(II)-treated $A\beta_{42}$ aggregates by 12 h incubation with Cyt *c* in the absence and presence of H_2O_2, and cells were incubated with the resultant aggregates for 24 h, as depicted in Fig. 5. Cyt *c* with and without H_2O_2 generated metal-free $A\beta_{42}$ aggregates that showed less cytotoxicity by approximately 15% and 7%, respectively, than those untreated with either Cyt *c*, H_2O_2, or both. In the case of preformed Zn(II)–$A\beta_{42}$ aggregates, cell viability was improved by about 6% and 20%, respectively,

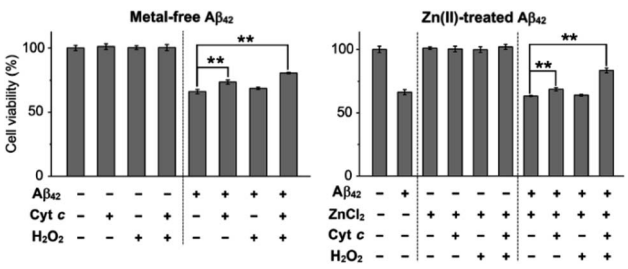

Fig. 5 Influence of Cyt *c* on the cytotoxicity induced by metal-free and Zn(II)-treated $A\beta_{42}$ species with and without H_2O_2. SH-SY5Y cells were treated with metal-free and Zn(II)-added $A\beta_{42}$ species generated by 12 h treatment with either Cyt *c*, H_2O_2, or both followed by 24 h incubation. Cell viability, determined by the MTT assay, was calculated in comparison to that with an equivalent amount of the buffered solution. Conditions: $[A\beta_{42}] = 10\ \mu M$; [Cyt *c*] = 10 μM; $[Zn(II)] = 10\ \mu M$; $[H_2O_2] = 80\ \mu M$; 150 mM HEPES, pH 7.4. Data are represented as mean ± s.e.m. $^{**}P < 0.01$ by Student's *t*-test.

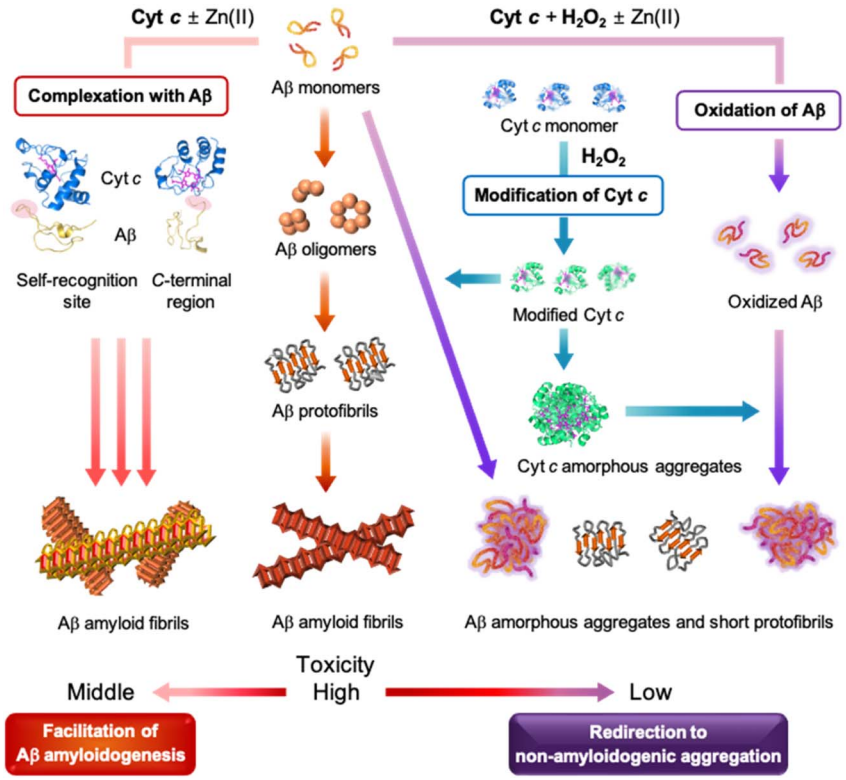

Fig. 6 Potential mechanisms for the impact of Cyt *c* on Aβ aggregation in the absence and presence of H_2O_2. Cyt *c* facilitates Aβ aggregation through their adduct formation in the absence of H_2O_2. Upon incubation of Cyt *c* with Aβ in the presence of H_2O_2, off-pathway amorphous and less toxic Aβ aggregates are generated by three possible mechanisms, including (i) the complexation between Cyt *c* and Aβ, (ii) the oxidation of Aβ by Cyt *c* and H_2O_2, and (iii) the modification of Cyt *c* induced by H_2O_2.

with addition of Cyt *c* in the absence and presence of H_2O_2. These results illustrate that the aggregates of metal-free $A\beta_{42}$ and Zn(II)–$A\beta_{42}$ produced with Cyt *c* have distinct cytotoxicity depending on the presence of H_2O_2, which is supported by the aggregation studies described in Fig. 1. Notably, amorphous metal-free and Zn(II)-treated $A\beta_{42}$ aggregates obtained with both Cyt *c* and H_2O_2 shown in Fig. 1C were less toxic than those with either Cyt *c* or H_2O_2 and without both. It should be noted that the amounts of Cyt *c* and H_2O_2 used for cell studies did not cause cytotoxicity under our experimental conditions (Fig. S21†). Our cell and aggregation results suggest the regulatory reactivity of Cyt *c* towards the aggregation and toxicity of Aβ particularly in the presence of ROS.

Conclusions

Cyt *c* is a crucial protein that influences various cellular processes linked to respiration, apoptosis, and redox signalling and, thus, is highly relevant to the development of neurodegenerative diseases such as AD.[13,14,43] Recent findings suggest the reactivity of Cyt *c* with Aβ;[20–22] however, details on whether and how Cyt *c* affects the aggregation and toxicity of Aβ are not known thus far. Through our investigations, we demonstrate, *for the first time*, that Cyt *c* can modulate the amyloidogenesis of both metal-free Aβ and metal-bound Aβ in a peroxide-dependent manner, to the best of our knowledge. Our findings contribute to a deeper understanding of the relationship between Cyt *c* and the aggregation and toxicity of Aβ, which may have important implications for the prevention and treatment of AD.

Our comprehensive studies shed light on the influence of Cyt *c* on the size distribution, morphology, and secondary structures of both metal-free Aβ and Zn(II)–Aβ to different extents. Our results illustrate that the presence of ROS such as H_2O_2 changes the impact of Cyt *c* on Aβ amyloidogenesis. As summarized in Fig. 6, Cyt *c* accelerates Aβ peptides into amyloids, while in the presence of H_2O_2, it redirects Aβ peptides into less toxic off-pathway aggregates. These effects are observed regardless of the presence of Zn(II) and may be driven by a combination of possible mechanisms: (i) the complexation between Cyt *c* and Aβ, (ii) the oxidation of Aβ by Cyt *c* and H_2O_2, and (iii) the modification of Cyt *c* by H_2O_2. Our experimental studies with computer simulations support that Cyt *c* directly interacts with the self-recognition and C-terminal regions of Aβ that are critical for Aβ aggregation,[2,4] in a relatively weak binding manner, which results in facilitating Aβ amyloid formation. Furthermore, Cyt *c* with H_2O_2 promotes oxidative modifications onto the His14 and Met35 residues in Aβ and, thus, alters its aggregation behavior. Lastly, amorphous Cyt *c* aggregates are formed in the presence of H_2O_2, consistent with previously reported studies,[31,40] which can notably modify the aggregation of Aβ. The aggregation of metal-free and Zn(II)-bound Aβ in the absence and presence of Cyt *c* and H_2O_2 is highly complex, involving the generation of diverse

aggregates at intermediate incubation time points. Future investigations would be valuable to elucidate the physiological and pathological activities of intermediate aggregates in biological systems. Our work validates the novel protective of Cyt *c* in Aβ amyloidogenesis and demonstrates its ability to modulate the aggregation and toxicity profiles of both metal-free and metal-bound Aβ.

Data availability

All experimental details and data supporting the findings of this study are available within the paper and its ESI.† The data are also available from the corresponding authors upon reasonable request.

Author contributions

Z. D., Y.-H. L., and M. H. L. designed the research. Z. D. and E. N. performed CD, TEM, ESI-MS, UV-Vis, biochemical assays, and cell studies with data analyses. Y. L. and Y.-H. L. conducted 2D ^{1}H–^{15}N NMR, ITC, and DLS experiments and analyzed the data. M. H. and M.-H. B. carried out MD simulations with analysis. T. M. performed the expression and purification of ^{15}N-labeled recombinant $A\beta_{42}$ and K. I. provided ^{15}N-labeled Cyt *c*. Z. D., E. N., M. H., and M. H. L. wrote the manuscript with input from all authors.

Conflicts of interest

There are no conflicts to declare.

Acknowledgements

This work was supported by the National Research Foundation of Korea (NRF) grant funded by the Korean government [NRF-2022R1A3B1077319 (M. H. L.); NRF-2019R1A2C1004954 and NRF-2022R1A2C1011793 (Y.-H. L.)]; National Research Council of Science & Technology (NST) grant funded by the Korean government [CCL22061-100 (Y.-H. L.)]; KBSI fund (C320000, C330130, and C390000) (Y.-H. L.); the Institute for Basic Science (IBS-R010-A1) in Korea (M.-H. B.); the Grant-in-Aid for Scientific Research on InnovTive Areas (19H05769) (K. I.); National Research, Development and Innovation Fund of Hungary [K138937 and 2018-2.1.17-TÉT-KR-2018-00008 (T. M.)]. We thank Professor József Kardos (Eötvös Loránd University, Hungary) for providing ^{15}N-labeled recombinant $A\beta_{42}$.

References

1 I. W. Hamley, *Chem. Rev.*, 2012, **112**, 5147–5192.
2 K. P. Kepp, *Chem. Rev.*, 2012, **112**, 5193–5239.
3 M. G. Savelieff, G. Nam, J. Kang, H. J. Lee, M. Lee and M. H. Lim, *Chem. Rev.*, 2019, **119**, 1221–1322.
4 S. J. Lee, E. Nam, H. J. Lee, M. G. Savelieff and M. H. Lim, *Chem. Soc. Rev.*, 2017, **46**, 310–323.
5 J. Han, Z. Du and M. H. Lim, *Acc. Chem. Res.*, 2021, **54**, 3930–3940.
6 D. A. Butterfield, A. M. Swomley and R. Sultana, *Antioxid. Redox Signaling*, 2013, **19**, 823–835.
7 L. Zuo, B. T. Hemmelgarn, C. C. Chuang and T. M. Best, *Oxid. Med. Cell. Longevity*, 2015, **2015**, 604658.
8 C. Cheignon, M. Tomas, D. Bonnefont-Rousselot, P. Faller, C. Hureau and F. Collin, *Redox Biol.*, 2018, **14**, 450–464.
9 E. Atrian-Blasco, P. Gonzalez, A. Santoro, B. Alies, P. Faller and C. Hureau, *Coord. Chem. Rev.*, 2018, **375**, 38–55.
10 P. Faller, C. Hureau and O. Berthoumieu, *Inorg. Chem.*, 2013, **52**, 12193–12206.
11 K. J. Barnham, C. L. Masters and A. I. Bush, *Nat. Rev. Drug Discovery*, 2004, **3**, 205–214.
12 F. Collin, C. Cheignon and C. Hureau, *Biomarkers Med.*, 2018, **12**, 201–203.
13 R. Santucci, F. Sinibaldi, P. Cozza, F. Polticelli and L. Fiorucci, *Int. J. Biol. Macromol.*, 2019, **136**, 1237–1246.
14 D. Alvarez-Paggi, L. Hannibal, M. A. Castro, S. Oviedo-Rouco, V. Demicheli, V. Tortora, F. Tomasina, R. Radi and D. H. Murgida, *Chem. Rev.*, 2017, **117**, 13382–13460.
15 C. Garrido, L. Galluzzi, M. Brunet, P. E. Puig, C. Didelot and G. Kroemer, *Cell Death Differ.*, 2006, **13**, 1423–1433.
16 H. Liu, S. M. Sarnaik, M. D. Manole, Y. Chen, S. N. Shinde, W. Li, M. Rose, H. Alexander, J. Chen, R. S. Clark, S. H. Graham and R. W. Hickey, *Resuscitation*, 2012, **83**, 1491–1496.
17 K. Gonzalez-Arzola, A. Velazquez-Cruz, A. Guerra-Castellano, M. A. Casado-Combreras, G. Perez-Mejias, A. Diaz-Quintana, I. Diaz-Moreno and M. A. De la Rosa, *FEBS Lett.*, 2019, **593**, 3101–3119.
18 H. S. Kim, J. H. Lee, J. P. Lee, E. M. Kim, K. A. Chang, C. H. Park, S. J. Jeong, M. C. Wittendorp, J. H. Seo, S. H. Choi and Y. H. Suh, *Neuroreport*, 2002, **13**, 1989–1993.
19 S. Morais Cardoso, R. H. Swerdlow and C. R. Oliveira, *Brain Res.*, 2002, **931**, 117–125.
20 C. Ghosh, S. Mukherjee and S. G. Dey, *Chem. Commun.*, 2013, **49**, 5754–5756.
21 A. Sarkar, K. Sengupta, S. Chatterjee, M. Seal, P. Faller, S. G. Dey and A. Dey, *ACS Omega*, 2018, **3**, 13994–14003.
22 M. Seal, C. Ghosh, O. Basu and S. G. Dey, *J. Biol. Inorg. Chem.*, 2016, **21**, 683–690.
23 A. J. Heck and R. H. Van Den Heuvel, *Mass Spectrom. Rev.*, 2004, **23**, 368–389.
24 K. Sakamoto, M. Kamiya, T. Uchida, K. Kawano and K. Ishimori, *Biochem. Biophys. Res. Commun.*, 2010, **398**, 231–236.
25 P. H. Nguyen, A. Ramamoorthy, B. R. Sahoo, J. Zheng, P. Faller, J. E. Straub, L. Dominguez, J. E. Shea, N. V. Dokholyan, A. De Simone, B. Ma, R. Nussinov, S. Najafi, S. T. Ngo, A. Loquet, M. Chiricotto, P. Ganguly, J. McCarty, M. S. Li, C. Hall, Y. Wang, Y. Miller, S. Melchionna, B. Habenstein, S. Timr, J. Chen, B. Hnath, B. Strodel, R. Kayed, S. Lesne, G. Wei, F. Sterpone, A. J. Doig and P. Derreumaux, *Chem. Rev.*, 2021, **121**, 2545–2647.
26 G. J. Morgan, *Biophys. Chem.*, 2022, **281**, 106711.
27 P. H. Nguyen and P. Derreumaux, *Biophys. Chem.*, 2020, **264**, 106421.

28 G. W. Bushnell, G. V. Louie and G. D. Brayer, *J. Mol. Biol.*, 1990, **214**, 585–595.
29 W. Yang, B. S. Kim, Y. Lin, D. Ito, J. H. Kim, Y.-H. Lee and W. Yu, *bioRxiv*, preprint, 2021, 2021.2008.2023.457317, DOI: **10.1101/2021.08.23.457317**.
30 N. T. Moldogazieva, I. M. Mokhosoev, N. B. Feldman and S. V. Lutsenko, *Free Radical Res.*, 2018, **52**, 507–543.
31 V. Yin, G. S. Shaw and L. Konermann, *J. Am. Chem. Soc.*, 2017, **139**, 15701–15709.
32 J. Han, H. J. Lee, K. Y. Kim, G. Nam, J. Chae and M. H. Lim, *Proc. Natl. Acad. Sci. U. S. A.*, 2020, **117**, 5160–5167.
33 J. Dong, C. S. Atwood, V. E. Anderson, S. L. Siedlak, M. A. Smith, G. Perry and P. R. Carey, *Biochemistry*, 2003, **42**, 2768–2773.
34 C. S. Atwood, X. Huang, A. Khatri, R. C. Scarpa, Y. S. Kim, R. D. Moir, R. E. Tanzi, A. E. Roher and A. I. Bush, *Cell. Mol. Biol.*, 2000, **46**, 777–783.
35 L. Hou, I. Kang, R. E. Marchant and M. G. Zagorski, *J. Biol. Chem.*, 2002, **277**, 40173–40176.
36 A. S. Johansson, J. Bergquist, C. Volbracht, A. Paivio, M. Leist, L. Lannfelt and A. Westlind-Danielsson, *Neuroreport*, 2007, **18**, 559–563.
37 L. Triguero, R. Singh and R. Prabhakar, *J. Phys. Chem. B*, 2008, **112**, 7123–7131.
38 C. Hureau and P. Faller, *Biochimie*, 2009, **91**, 1212–1217.
39 N. Tomaskova, P. Novak, T. Kozar, M. Petrencakova, D. Jancura, G. Yassaghi, P. Man and E. Sedlak, *Int. J. Biol. Macromol.*, 2021, **174**, 413–423.
40 N. H. Kim, M. S. Jeong, S. Y. Choi and J. H. Kang, *Mol. Cells*, 2006, **22**, 220–227.
41 M. Hashimoto, A. Takeda, L. J. Hsu, T. Takenouchi and E. Masliah, *J. Biol. Chem.*, 1999, **274**, 28849–28852.
42 M. Saxena, Y. Delgado, R. K. Sharma, S. Sharma, S. Guzman, A. D. Tinoco and K. Griebenow, *PLoS One*, 2018, **13**, e0195542.
43 A. Guerra-Castellano, I. Marquez, G. Perez-Mejias, A. Diaz-Quintana, M. A. De la Rosa and I. Diaz-Moreno, *Int. J. Mol. Sci.*, 2020, **21**, 8483–8502.